

## Frequency-enhanced imaging of stratigraphically complex, thin-bed reservoirs: A case study from South Marsh Island Block 128 Field

MARCUS L. COUNTISS, Pogo Producing Company, Houston, Texas, U.S.

Application of a poststack processing method that separates signal from noise, while enhancing only the high frequency "earth signal," helped identify new well locations in thinly bedded reservoirs that would not have otherwise been drilled. More importantly, wells drilled after application of this method added significant new reserves to a 27-year-old, offshore Gulf of Mexico field and nearly quadrupled daily production rates.

Numerous attempts have been made to image thin beds (<1/4 of dominant wavelength) by extracting higher frequencies from poststack seismic. Two common goals are: (1) define pinch outs of producing zones and (2) resolve internal bed geometries (lithofacies). This improved resolution is required during reservoir development. The most common poststack method is spectral whitening or boosting the amplitudes of all frequencies within a certain band-pass to the same level. The problem with this method is that it fails to discriminate noise from signal. Noise is boosted along with subsurface signal and, depending on the signal-to-noise ratio (SNR), may fail to extract the desired information. Other techniques such as coherence cube technology and seismic inversion help define some properties through a different approach but are limited by the inherent bandwidth of standard seismic.

**Case study—South Marsh Island.** The discovery well for South Marsh Island Block 128 Field (Figure 1) was drilled in June 1974. The field is a stratigraphically complex, salt-cored, NW-SE trending anticline bounded on the west by a large down-to-the-west fault. The reservoir ranges in age from Angulogerina B (Early Pleistocene), to Lenticulina 1 (Late Pliocene), and lies between 4500 and 9000 ft subsea. Original depositional bathymetry encompasses inner neritic paleo depths at the younger, shallower horizons, to upper bathyal, in deeper zones. All reservoirs are normally pressured. At the beginning of this project the field had seven exploratory wells and 93 platform wells, including sidetracks, drilled from four platforms. As of January 2000, cumulative production was 115 billion bbls of oil and 203 billion ft<sup>3</sup> of gas. Average daily production rates were 3500 bbls of oil and four million ft<sup>3</sup> of gas per day.

Structural interpretation had been difficult from the initial phase of interpretation. Various interpreters produced different structural pictures. Uncertainties about the amount of faulting persisted even after the acquisition of a proprietary, first generation 3D in 1989. Geoscientists working the field were aware of stratigraphic variations between wells but could not visualize the true level of depositional complexity using available seismic. Many reservoir units were below standard seismic resolution and impossible to map reliably. Distinguishing between faulting and stratigraphic discontinuities was problematic at best. This led to interpretation of complex fault patterns that were suspiciously "un-geologic."

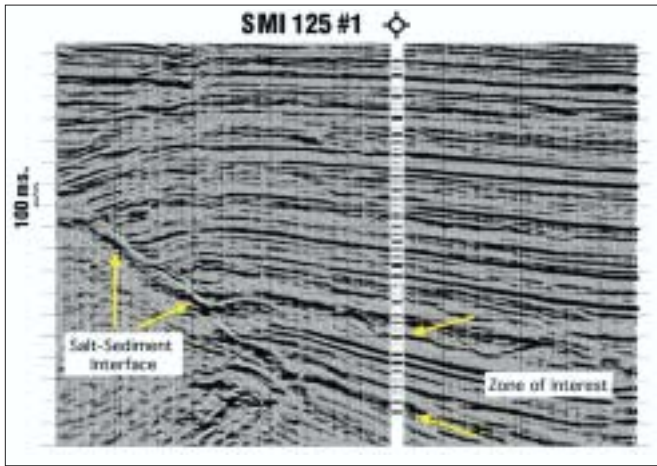


Figure 1. South Marsh Island 128 Field in the Gulf of Mexico offshore.

A 1994 vintage speculative 3D data set was reprocessed in early 1998, employing target-oriented, prestack Kirchhoff time migration in an attempt to resolve some of these issues. Field acquisition employed a 4000-m streamer with 25-m group and shot intervals, a 4-ms sample rate, and an 8-s record length. A 15 000-ft migration aperture was selected to optimize imaging.

Overall imaging was greatly improved leading to the conclusion that many discontinuities previously interpreted as faulting were, in fact, stratigraphic changes. Pressure data supported the fact that certain wells were in separate compartments, but this was still not clearly imaged in the 3D seismic. In hope of resolving these stratigraphic details, a poststack frequency enhancement routine was applied to the reprocessed data. This trademarked technique is called HFI. This technique employs a branch of mathematics originally developed in quantum mechanics for treating technically unsolvable systems (also called undetermined equations), in combination with equations derived for decoding of encrypted messages. After all, an encrypted message is essentially what the seismic trace is. For a more complete discussion of how the algorithm works, refer to the appendix at the end of this article.

**Calibration of data.** Criteria dictated that velocity and density data for synthetic generation be available and of good quality. Two wells were selected as calibration wells. Velocity survey information was incorporated. Logs were carefully edited by experienced petrophysicists to compensate for washouts, cycle skipping, and any other problems. The consequent reflectivity series were convolved with various high-frequency, band-pass wavelets to produce synthetic seismograms. These served as calibration points and quality control for the processing. The synthetic traces were compared to the data to optimize parameters of the high-frequency data volume. Figure 2 shows an in-line from the 3D volume at standard frequency with 8-30 Hz synthetic



**Figure 2.** In-line from 3D volume that ties directly the SMI 125 1 control well. Normal incident synthetic seismogram generated with 5-8-30-40 Hz band-pass wavelet is inserted at well tie point. Zone of interest bracketed by arrows. There are several distinctive reflectors on which the synthetic can be “hung” most notably about 100 ms below where the uppermost yellow arrow points. With a little stretch and squeeze in places the synthetic exhibits a good tie. Notice how well imaged the salt-sediment interface is.

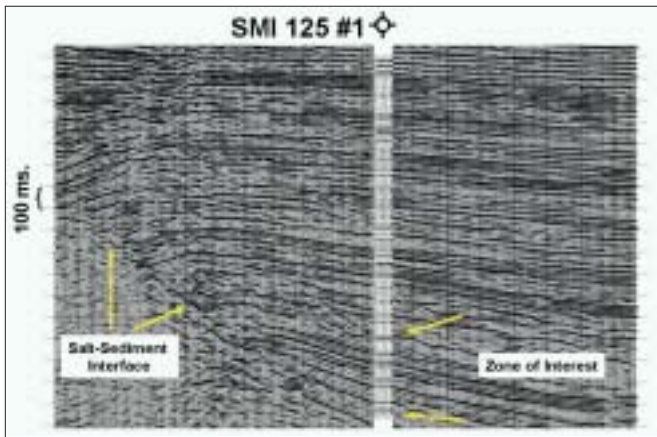


**Figure 3.** Final frequency-enhanced version of the in-line from Figure 2. Normal incident broadband (5-8-70-90 Hz band-pass) synthetic traces are inserted at tie point. AVO effects account for the apparent poor correlation in the first 200 ms of the synthetic, but the correlation in the target zone is quite good. The salt-sediment interface reflection is still present in this version, but not nearly as obvious as in the standard frequency data of Figure 2. The standard frequency version is still useful for gross structural definition.

traces inserted at the calibration well tie point. Note the nicely imaged salt-sediment interface in the lower left of the profile. Good correlation at this control point between the data and the synthetic seismogram at normal frequency showed us that the data quality was good enough to achieve success with frequency enhancement.

The high-frequency, mathematical imaging technique was then applied to the data set. The algorithm was allowed to run without imposed limits and boost frequencies to near Nyquist limits. At frequencies approaching 120 Hz, nongeologic “artifacts,” or events not correlative to the log-generated synthetic traces, appeared in the data. Therefore, data were filtered back to the point at which these artifacts disappeared (around 80 Hz). The resultant high-frequency data set was then compared to an 8-70 Hz broadband synthetic to evaluate the final version of the data. Reasonably good correlation was achieved at most levels with especially good matches in the target interval. Figure 3 illustrates the remark-

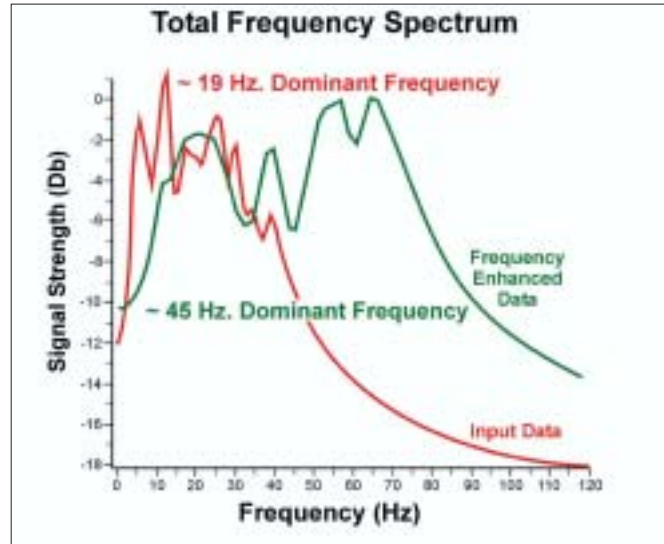


**Figure 4.** Comparison of frequency spectra before and after application of frequency-enhancement technique. The dominant frequency is calculated as the average frequency between the -6 dB slope points on either end of the spectrum.

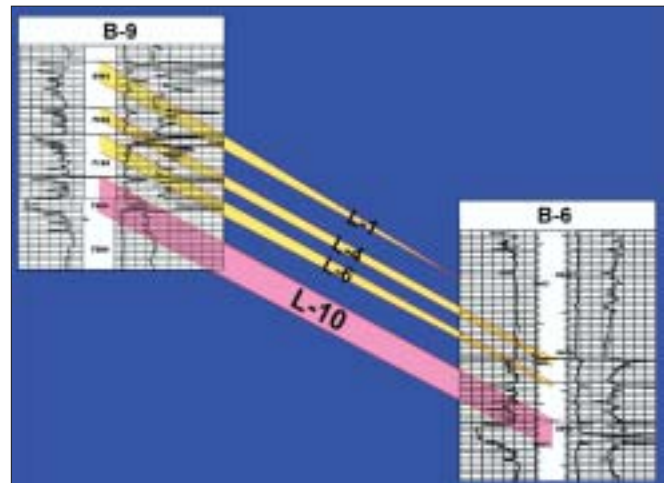


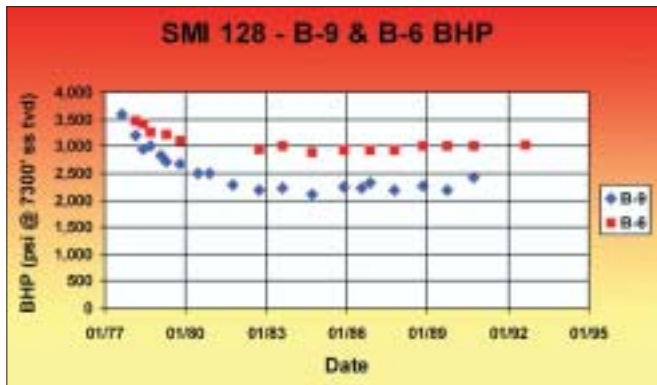
**Figure 5.** First generation subsurface cross-section showing correlation between wells B-6 and B-9. The L-10 subject horizon is red. This is primarily a simple subsurface log correlation.

able improvement in the frequency content of the data when compared to the input data.

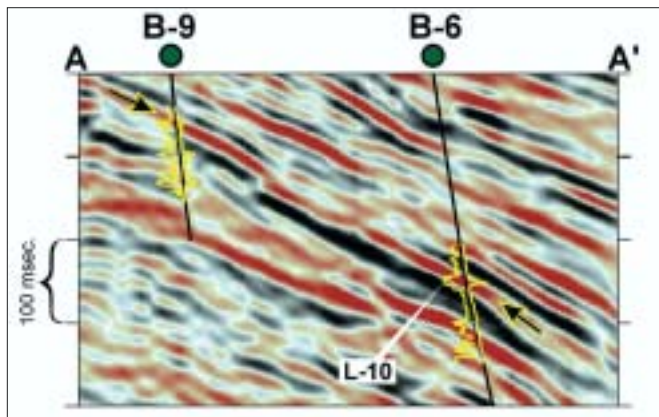
Gross structural features such as this salt-sediment event continue to be best delineated using the standard seismic volume. Look at the salt sediment interface highlighted in Figure 2. Although the event is still clearly visible in this frequency-enhanced version, it is fair to say that it is more “interpretable” in the standard frequency version.

Figure 4 shows the before-and-after frequency spectra from the target interval. Before application of the frequency enhancement, the dominant frequency was about 19 Hz. The frequency-enhanced version exhibits more than double the frequency content, increasing the dominant frequency to about 45 Hz. This data volume was integrated with well data to identify and evaluate new drilling targets. Acoustic impedance inversion supported the results and, in some cases, was a determining factor for one of the partners.

**A puzzling sand correlation and production problem.** In June 2000, the partners initiated a multiwell drilling program to test some identified opportunities. Let’s focus on the



**Figure 6.** Chart comparing BHPs from the L-10 reservoir in B-6 and B-9. The pressure profiles begin to diverge after one year of production. Note that the updip B-9 waters out in September 1991 while the downdip B-6 continues to produce until April 1994.



**Figure 7.** Standard bandwidth 3D arbitrary profile (A-A') connecting B-9 and B-6. Arrows indicate the reflector under investigation. SP log tracts appear to the left of the well bore projections with resistivity to the right. Red represents negative coefficients on the seismic color bar. The indicated reflector is essentially continuous between wells.

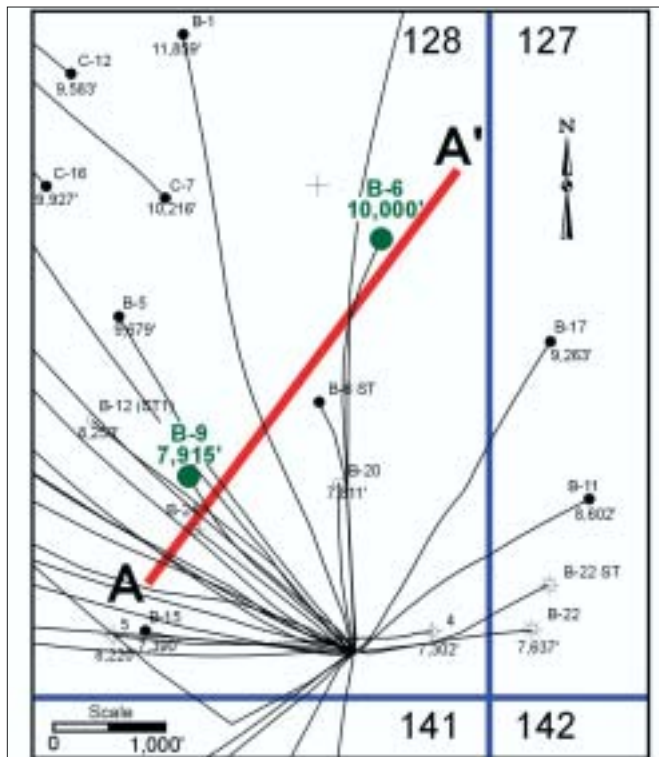


**Figure 8.** Map of the deviated well paths in South Marsh Island 128 Field showing the location of transect A-A'.

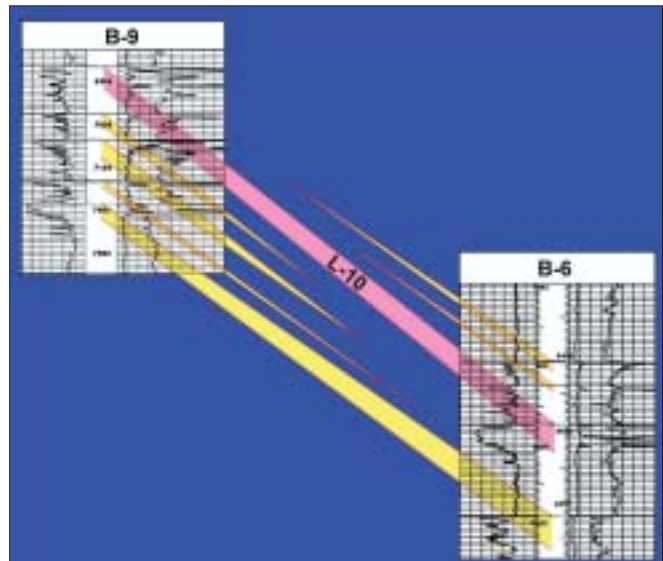


**Figure 9.** Revised subsurface cross-section based on standard bandwidth 3D seismic. Note increased complexity of correlations compared to Figure 5. This stratigraphy seems more likely given the depositional environment and lobe shifting sedimentation style.

results of two wells drilled early in the development of SMI 128 Field. Well B-6, drilled in the southern portion of the field in April 1976, encountered 47 ft of net oil pay in two zones. B-9, drilled 2300 ft to the southwest of the B-6 in June 1976, encountered 149 ft of net oil pay in four zones. Both are directional platform wells drilled into generally east dipping strata, with no water contacts encountered by either well in any pay zone.

As an example, we are going to concentrate on a reservoir referred to as the L-10 zone, a Lentic 1 age horizon. The first generation interpretation (Figure 5) shows a subsurface log cross-section between wells B-6 and B-9 connecting all L series sands (L-1 through L-10). Note that the L-1 zone in the updip B-9 well is interpreted to be absent in the downdip B-6 well. All other L series horizons (L-4, 6, and 10) are shown to be continuous except for variations in thickness and character. This turned out to be a rather simplistic interpretation because we later realized the sand was deposited in an upper bathyal environment where rapid lobe shifting took place. In any case, this correlation was generally accepted (with small variations) by the partners during the early stages of field development. However, after years of production, the bottom-hole pressure (BHP) profiles show a divergent trend between these two zones, demonstrating that they could not be in communication with each other. Figure 6 illustrates this comparison. Furthermore, the L-10 zone (-7021 SSTVD) in B-9 watered out in September 1991 after producing over 2 million bbls of oil and 2369 million ft<sup>3</sup> gas. The L-10 completion (-7587 SSTVD) in B-6 continued to produce until watering out in April 1994 after recovering 539 000 bbls of oil and 690 million ft<sup>3</sup> gas. How can the fact that the updip well watered out before the downdip well be reconciled? Clearly some type of separation exists, but can it be defined with seismic data?

Before application of the frequency-enhancement technique, the standard frequency reprocessed version of the 1994 vintage speculative 3-D data (Figure 7) was employed to further advance the accuracy of reservoir correlations. Figure 8 shows the location of this transect (A-A'). It directly connects the L series interval in B-6 and B-9 with SP and resistivity log curves overlain on the data. Arrows indicate the event representing L-10. Note that the reflector is essentially continuous between B-6 and B-9. Furthermore, corre-

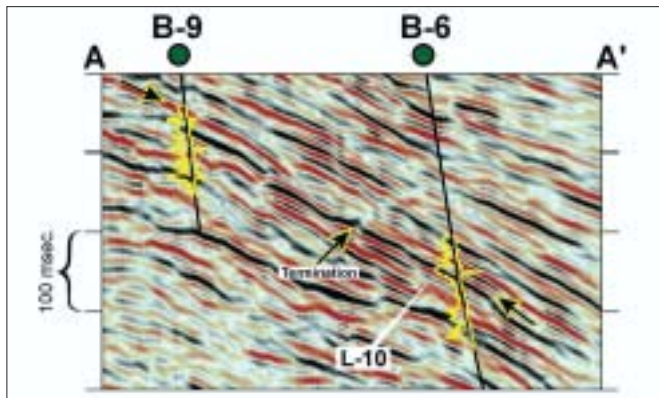


Figure 10. The same traverse (A-A') in Figure 4 shown in high frequency. Dominant frequency is roughly 45 Hz. Arrows indicate equivalent reflector to Figure 4. Reflector termination is also shown by arrow. Primary reservoir units now appear to have top and base events.

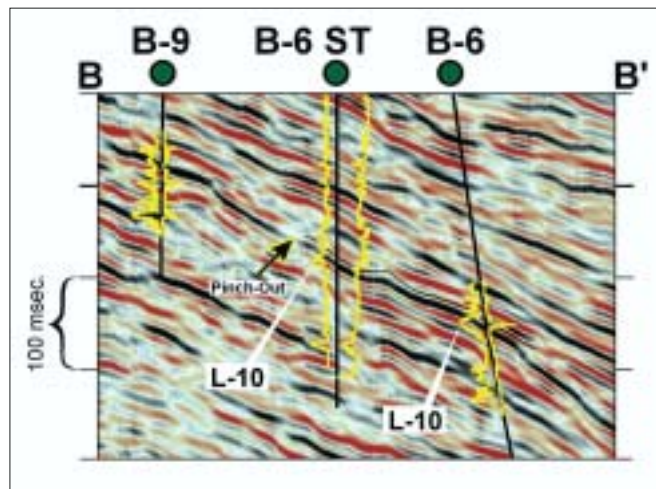


Figure 12. A high-frequency profile (B-B') incorporating newly drilled well B-6 ST. B-6 ST posts at the bend in the arbitrary profile (see Figure 13). The L-10 reflector is tracked by the black line and the stratigraphic separation (pinch out) is highlighted by the arrow.

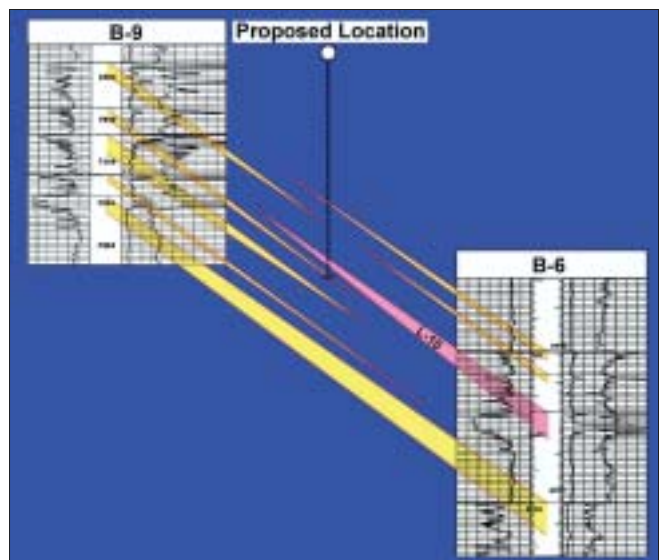


Figure 11. Revised subsurface cross-section based on frequency-enhanced 3D seismic. Compare with Figure 9. The proposed location targets an apparent undrained attic reserve updip to B-6.

lations from B-6 have shifted shallower relative to B-9. This leads to a revised cross-section (Figure 9). Maintaining the original nomenclature for the reservoirs, the L-4 and L-6 zones in B-6 are now shown not present in B-9. More importantly, the L-10 zone of interest ties to a continuous reflector that now connects it to what was L-1 in B-9. Further review indicates that there is a pressure difference of more than 1000 psi between these two zones, implying that they cannot be in the same reservoir. Once again the standard bandwidth seismic failed to resolve the correlation.

**Seismic resolution solution using high-frequency data.** The objective is to image a zone that, according to logs, is on the order of 20-40 ft gross thickness. Although the data quality is very good, interpretation is limited by the inherent bandwidth of the data. The dominant frequency in the zone of interest is roughly 19 Hz, as noted previously (Figure 4). Interval velocity is 8850 ft/s, making the dominant tuning thickness about 116 ft (1/4 wavelength). Even at the upper end of the available spectrum of ~28 Hz, the thinnest possible discrete resolution is 79 ft. A reflection at the top of the zone may be expected but imaging the base is not achievable and, due to bandwidth limitations, not resolvable as a separate seismic event. The pay is not associated with a classic bright spot so an amplitude extraction does little to reveal any reservoir

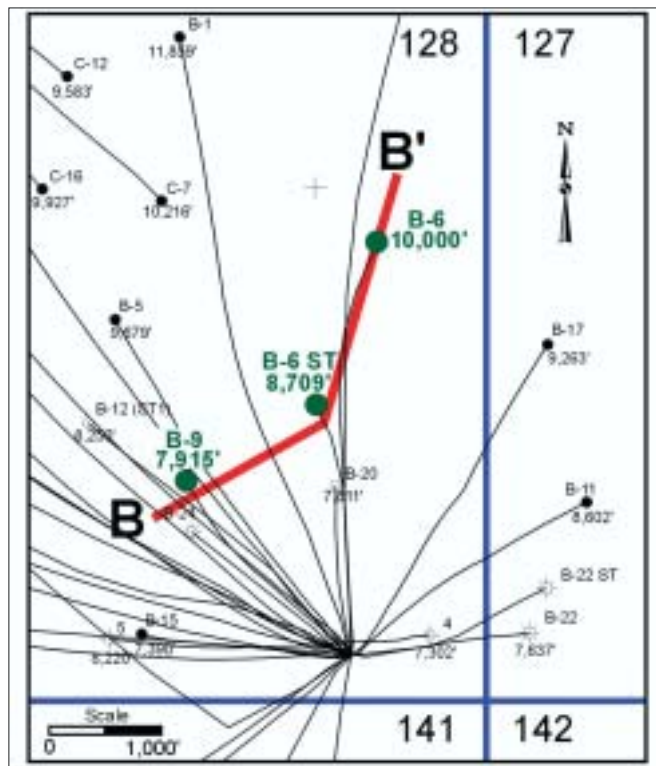
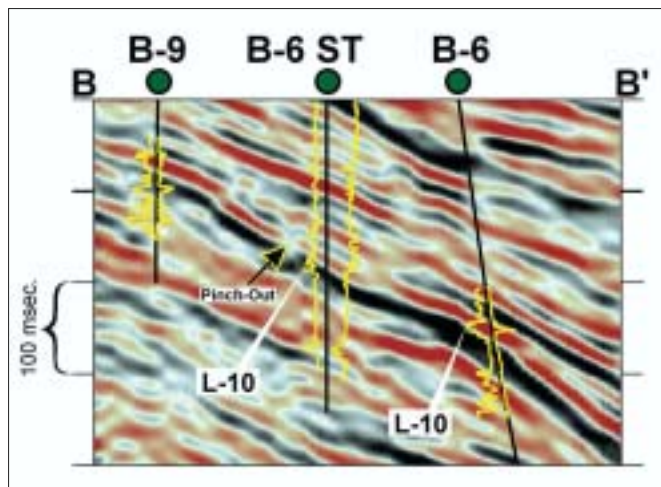


Figure 13. Location of transect B-B'. The new B-6St well track is also posted.

boundaries. In addition, the 3D suggests that the separation is not fault related. Yet pressure and production data indicate that production is from two separate reservoirs. The separation must be stratigraphic. It was at this point that the high-frequency version of the 3D data set was applied to see if it could image what was believed to exist.

Figure 10 is the same A-A' arbitrary line shown in Figure 7 except that the frequency enhancement technique has been applied. The dominant frequency is now nearly 45 Hz, making the tuning thickness roughly 49 ft. The upper end signal frequencies, however, extend to 80 Hz making the resolution of beds as thin as 27 ft possible. The individual reservoir units now tie to discrete events on the seismic with top and base reflections observable in most cases. The top of the zone of interest is again indicated by the arrows. Note that the event



**Figure 14.** The same profile (B-B') as in Figure 9, but in the standard bandwidth format. The stratigraphic separation is still imaged in the particular view. This separation is not laterally continuous when viewed with the standard frequency 3D volume.

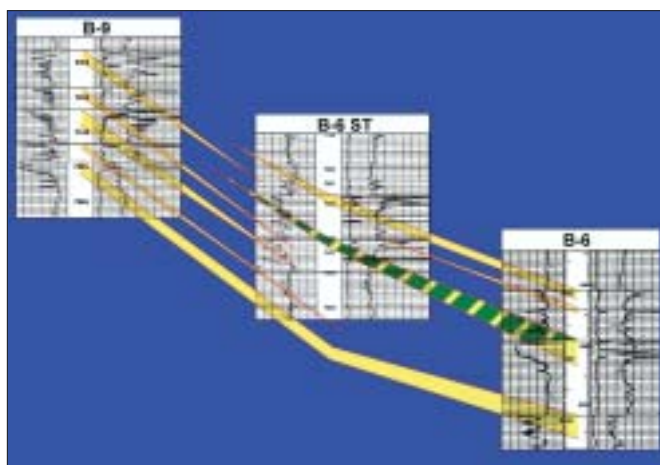


**Figure 15.** Final cross-section incorporating newly drilled B-6 sidetrack. The L-10 additional oil reservoir, proved by B-6 ST, is shown by the yellow and green hatched area. Two additional hydrocarbon accumulations occur above the L-10 unit, as evidenced by the resistivity response on the log, that are not productive in B-6.

that ties the L-10 zone in B-6 appears to have a break or termination before it reaches B-9. It was interpreted as a stratigraphic pinch out and demonstrates the separation indicated by the pressure and production data. Geologically, the L series sands were deposited in an upper slope environment, based on paleontology. Sedimentation rates were high, and there was a very rich sand source. As sediment was deposited, feeder channels shifted rapidly like water coming out of a fire hose, filling depositional lows. Syn-depositional salt movement accentuated this, creating a complex, interfingered system of sand bodies. Realization of this complexity prompted another generation of cross-sections (Figure 11) that honor the apparent correlation revealed by the high-frequency data. This version exhibits more stratigraphic discontinuity than any previous interpretation, but fits with the depositional history. It also offers an interpretation that reconciles the pressure and production history. Is this coincidence or truly the product of higher seismic resolution?

**Sidetrack confirms new correlation based on seismic.** A detailed review of the new cross-section (Figure 11) revealed an apparent, undrained reservoir in the zone of interest. Because the L-10 zone in B-6 was productive and after find-

ing that the reservoir can be penetrated updip to the B-6 take point, without a break in continuity, led to the conclusion that a new drilling target had been defined. In November 2000, a sidetrack of B-6 was spudded to test the prospect. The well reached total depth and logged in early December 2000. Logs revealed oil pay in three zones for a total of 52 ft of net oil pay—26 ft was in the L-10 zone of interest, with no water contact present. Independent engineering calculations assigned 407 000 bls of oil and 183 million ft<sup>3</sup> gas of new proved reserve additions to the field with 203 000 bls of oil coming from the zone of interest.

Figure 12 shows a frequency-enhanced 3D transect (B-B') that incorporates the new B-6 ST with B-6 and B-9. Figure 13 shows the location of this transect. Again the target horizon is indicated in the B-6 and the new B-6ST wellbores with the black line tracking the seismic event related to the horizon. The discontinuity marked by the arrow separates B-6 and B-6ST from the updip B-9. This agrees with the separation implied by the pressure data. Figure 14 shows the normal bandwidth version of this line. The discontinuity discovered on the frequency-enhanced version is also apparent on this particular profile (highlighted by the arrow) albeit in a less obvious state. Clearly there are places where the separation is visible on the standard bandwidth seismic but this is something that was never apparent in previous investigations by this author. This break in the reflector certainly does not appear on the profile in Figure 7 and is laterally discontinuous when viewed in detail. In any event, this prospect was never previously identified. This finally leads to the cross-section incorporating B-6ST (Figure 15) which shows the correlation supported by the high-frequency data.

**Conclusion.** In summation, this project generated seven new drilling opportunities, all commercial producers. It would be misleading to claim that all these wells were primarily the product of high-frequency imaging. Two were essentially production acceleration wells although frequency-enhanced data helped optimize the target locations. One was a sidetrack of an existing well that had a completion failure and was drilled back into the same zone. The remaining four wells relied principally on the high-frequency data and acoustic impedance inversion. Only one well had to be sidetracked to obtain a positive result, and this well was completed in a secondary target as a commercial producer. This could be counted as a failure because the primary target was noncommercial. However, six out of seven was deemed an acceptable success rate for any method employed. As of May 2001, total daily field production rates averaged 11 500 bls of oil and 18 million ft<sup>3</sup> of gas, a 328% increase in oil rates and a 450% increase in natural gas rates! Furthermore, an estimated 3.5 million bls of oil and 5 billion ft<sup>3</sup> gas of proved reserves were added to the field. Not a bad day's work in a 27-year-old field!

Because the frequency-enhancement technique was applied as a poststack process, it is very important that prior processing of the data set be state of the art. Accurate statics, velocities, and migration must be applied because errors in these steps affect high frequencies more than low frequencies. Favorable results were obtained in the example presented because basic data quality was good, but inferior acquisition and processing may restrict or eliminate the effectiveness of the method. Although the clear success of the drilling program supports the validity of the method, good matches with broadband synthetics demonstrate the ability of the technique to extract real high-frequency signal. As with all seismic methods, this not a "silver bullet" that will achieve all goals, but it is another weapon in the seismic arsenal. Application of the AI (acoustic inversion) inversion of the high-frequency data

set has not been detailed in this paper, but it was beneficial in the course of this program.

**Appendix.** The algorithm works to decode the seismic “message” and extract the reflectivity series directly from it. The process approaches the convolution of the “earth signal” or reflectivity series with the source, receiver, instrumentation etc. signatures (embedded wavelet) as an encoding matrix multiplication and vector rotation. The operation is entirely mathematical with no wavelet estimation or other interpretive input applied. The primary requirement is a seismic trace with reasonably good SNR. The predominant mind-set in our science treats the seismic signal as a convolution in the time domain, which is equivalent to multiplication of amplitudes in the frequency domain. Therefore, the output function contains only frequencies common to both of the input functions. This is referred to as “circular convolution” and does, in fact, filter the high frequencies rendering them unrecoverable. This, however, is not true of “one-sided convolution,” which occurs in the earth encoding process (the convolutional model of seismic data) and in the time-domain filtering during processing.

Consider the broadband reflectivity series, or “earth signal,” to be convolved with the band-limited embedded wavelet through the process of polynomial multiplication (one-sided convolution). It has been shown that the process of polynomial division exactly reverses the apparent band-limiting effects of convolution. For example, if one has convolved a set of reflection coefficients with a band pass filter to generate a synthetic seismic trace, then the original reflection series can be exactly recovered using polynomial division. For this to be successful, the entire synthetic trace must be input and there can be no noise or time variant filtering. If any of these rigid

conditions are not met, the direct solution becomes unstable and fails. Because actual seismic data violates all three requirements, this approach has been unsatisfactory on real-world examples. The method used here takes an alternative approach by describing one-sided convolution as a matrix multiplication with the problem resembling a process used to decode encrypted messages. Here the earth reflectivity is not filtered but “encoded” with the upper portion of the spectrum not removed but rather encrypted in the lower end of the spectrum which is still observable. This procedure views the seismic trace as the result of a matrix multiplication involving a square scrambling matrix with the rows composed of the time variant wavelet and a column matrix containing reflection coefficients. Given the unscrambling matrix, the message can be recovered. Even without the unscrambling matrix, code-breakers have developed iterative algorithms capable of recovering the message.

Matrix multiplication can be viewed as vector rotation in multidimensional space where time and frequency domains are just two of many. As previously stated, it has been usually assumed that the seismic wavelet filtered the earth reflectivity thus eliminating frequencies in the upper end of the spectrum. The apparent band-limiting effects of the one-sided convolutional model are viewed as a rotation of the reflectivity series vector away from the high-frequency coordinates toward the low-frequency coordinates. As this rotation proceeds, the magnitude of the reflection coefficient (RC) vector on each high frequency axis diminishes until it falls below the ambient noise. Ambient noise is thought of as being roughly spherical around the origin with components on all axes, assuming it is approximately flat across the frequency spectrum. Attempts to recover a frequency by directly scaling the vector component (spectral whitening or spiking deconvolution) amplify the signal and noise equally. By treating the seismic trace as a rotated vector, applying a reverse rotation increases the magnitude of the signal on the high-frequency coordinates without boosting ambient noise because its spherical nature tends to be invariant under such a rotation. Consequently, signal emerges from beneath the noise level and is recoverable. The projection of the resultant RC vector is very similar to the “earth signal” or unconvolved reflectivity series and produces a reasonable estimate of the reflectivity series with greater resolution than the input seismic trace. Because the entire spectrum is encoded by the embedded wavelet, it is theoretically possible to regain frequencies up to Nyquist on properly recorded and processed data. **TE**

*Acknowledgments: The author thanks Pogo Producing Co. and Devon Energy for their kind support. Special thanks to Geotrace Technologies for use of the HFI processing and WesternGeco for permission to publish data from its multiclient digital seismic library. Also, thanks to Carl Zinsser for technical guidance and Marsha Brown for outstanding graphic design. Assistance with engineering data provided by Bill Foshag of Pogo and Johnny Rau with Devon.*

Corresponding author: [countiss@pogoproducing.com](mailto:countiss@pogoproducing.com)

*Marc Countiss graduated with a BS in geology with geophysics option (1978) from the University of Houston. He is district geophysicist with Pogo Producing Co. in Houston, Texas, working both South Texas and offshore Gulf of Mexico. He worked for Gulf Oil E&P immediately after graduation and later Strata Energy, Inc. He spent several years as a consultant and independent prospect generator before joining Pogo in 1991. His professional interests are in exploration planning and play development, seismic sequence stratigraphy, and seismic attribute analysis.*